Deep-learning light-sheet fluorescence microscopy for high-throughput, voxel-super-resolved imaging of biomedical specimens

Hao Zhang[1], Chunyu Fang[1], Peng Fei[1,2,3*]

[1]School of Optical and Electronic Information, Huazhong University of Science and Technology, Wuhan, 430074, China.

[2]Britton Chance Center for Biomedical Photonics, Wuhan National Laboratory for Optoelectronics, Huazhong University of Science and Technology, Wuhan, 430074, China.

[3]Shenzhen Huazhong University of Science and Technology Research Institute, Shenzhen, 518000, China.

*Correspondence: feipeng@hust.edu.cn

Abstract

Light sheet fluorescence microscopy has recently emerged as a technique-of-choice for three dimensional mapping of biomedical samples such as large organs and whole embryos. Although it has great advantages over conventional wide-field microscopy because of its strong 3-D capacity, high speed and low phototoxicity, the imaging resolution of light-sheet fluorescence microscopy remains limited by many factors, such as the axial extent of plane illumination, the magnification of fluorescence detection, and light scattering from deep tissues. Here we present a computational approach that uses deep learning strategy to rapidly enhance the resolution of three-dimensional light-sheet fluorescence image. This deep-learning LSFM method achieves 1 μm^3 voxel resolution over 22 mm^3 volume without the need of either tile stitching or multi-frame super-resolution processing. Thus, it shows ultra-high throughput for volumetric imaging of whole organisms, quickly reconstructing tens of giga-voxel higher-resolution image based on simple acquisition of giga-voxel raw image using conventional low-magnification LSFM system. We demonstrate the success of this approach by imaging zebrafish heart and mouse brain tissue, 3-D visualizing massive cellular details across monolithic macro-scale samples.

Introduction

The emerging Light sheet fluorescence microscopy (LSFM) enables three dimensional (3-D) mapping of biomedical samples at relatively high speed and low phototoxicity [1-7]. By taking the advantage of a thin light-sheet illumination, LSFM can optically section the transparent biological samples, successively imaging a volume-of-interest plane by plane. Compared to the conventional epifluorescence methods, it significantly decreases the influence of out-of-focus excitation while reduce the photo-damage, obtaining high-contrast 3-D image at low photon burden. Therefore, the recent integration of LSFM with advanced tissue clearing techniques has become an important alternative to conventional histology/pathology imaging approaches, quickly interrogating the intact organs, such as hearts and brains, without the need of physically sectioning them into pieces [2, 3, 8-13]. However, the conflict between large field-of-view (FOV) and high resolution that exists in general microscopy does not make an exception in LSFM. Directly imaging of an entire large specimen requires thick laser-sheet illumination and low magnification detection to cover large FOV, at the expense of sacrificing high-frequency details which can only be captured under higher magnification. Tile imaging has been developed as a common solution which stitches multiple small volumes obtained under high magnification into a large one, to artificially increase the space-bandwidth product (SBP) of LSFM imaging. Despite the compromised speed induced by repetitive

mechanical stitching, the high magnification configuration in tile imaging induces increased phototoxicity for increasing sample size and limits fluorescence extraction from deep tissue. Several resolution enhancement techniques, such as Fourier ptychographic microscopy[14, 15], optical projection tomography[16, 17], optical diffraction tomography[18-22] and sub-voxel-resolving microscopy[11, 23, 24], have been reported as a computational means of reconstructing a wide-FOV, high-resolution (HR) 3-D image based on a number of low-resolution (LR) volumes having certain correlations in the space, frequency, or spectrum domain. However, these techniques still have limited imaging throughput caused by relatively increased acquisition time and complex computation procedure. Recently, neural network based approaches have shown their success in conventional 2-D microscopy for both bright-filed [25, 26] and fluorescence imaging [27-31], enhancing the spatial resolution of single large-FOV image at very high processing speed. This also indicates the strong potential of neural network to be pushed further for 3-D imaging with higher resolution and throughput.

Here we for the first time present a deep-learning based voxel-super-resolution (DVSR) technique and combine it with LSFM imaging, to improve the compromised image resolution caused by low magnification /NA optics as well as light scattering in thick tissues. This computational approach eliminates the need of any hardware retrofit to existing LSFM optics, employing efficient convolutional neural networks (CNNs) to perform the non-linear, volumetric mapping from single low-resolution measurement to a high-resolution output. The capability of our deep-learning LSFM (DLSFM) has been verified by imaging several thick samples, such as heart and brain tissues. As a reference point, it achieves a 4-time enhanced resolution of ~10 µm (compared to the original ~40 µm) throughout the large volume of an adult zebrafish heart (over 10 mm^3), at a low time cost of ~2 minutes. In the following, we introduce the implementation of the DV-LSFM imaging and demonstrate it applications to high-resolution, high-throughput organ mapping.

Results

Convolutional Neural Network based 3D super resolution

We aim to reconstruct a 3D image volume with abundant high frequency details from a low resolution LSFM image volume taken under a low magnification objective, of which the image quality is degraded due to an insufficient sampling rate and is highly corrupted by scattered light. Inspired by the success of CNN enabled 2D image super resolution[32-34], we designed DVSR, a deep-learning approach for restoring 3D super-resolution views from decimated LSFM images.

As all other deep learning approaches act, DVSR comprises a training stage and an inference stage (Fig. 1). At training stage, the neural network establishes its super-resolution ability from scratch by learning from a bunch of examples, where the low resolution LSFM image volumes are used as the input of the network, and high resolution volumes with the identical lateral FOV and axially spatial coverage as the target – which is the desired output of the network. We adhere to the practice of using an image degrading model[27] to generate simulated LR training data from HR LSFM measurements. Apart from the simplified training data acquisition process, an intrinsic drawback of LSFM make it necessary to do so. If both HR and LR training data were realistically obtained measurements of the sample to be mapped, the repeatedly light sheet scanning through the whole sample would bring severe bleach to the fluorescent signals, resulting in an inferior image acquisition with signal quality far under common practice. The use of the degrading model could avoid this by composing LR training data via simulation, reducing light sheet scanning times

as well as chances that the sample is bleached.

After LR simulations being generated, training of the network proceeds as follows. The LR is first fed to the network as the input, while the corresponding HR image volume is defined as the desired output. The network outputs the reconstruction of the input, which is rough and of low quality at first. We further define the pixel-wise mean square error (MSE) between this intermediate output and its target – the HR volume as the loss function, judging how well the current output matches the desired one. If considering the input and the target as constant, the loss is essentially a function of the parameters in the network. By iteratively minimizing the loss function using a gradient descent approach, the parameters of network get optimized gradually, enduing the network its ability to output a reconstruction with great image quality improvement. Once the training terminated, the network can be applied to a new LR measurement which is realistically captured by LSFM, and reconstruct a high-quality, super-resolved image volume (Fig. 1b, inference).

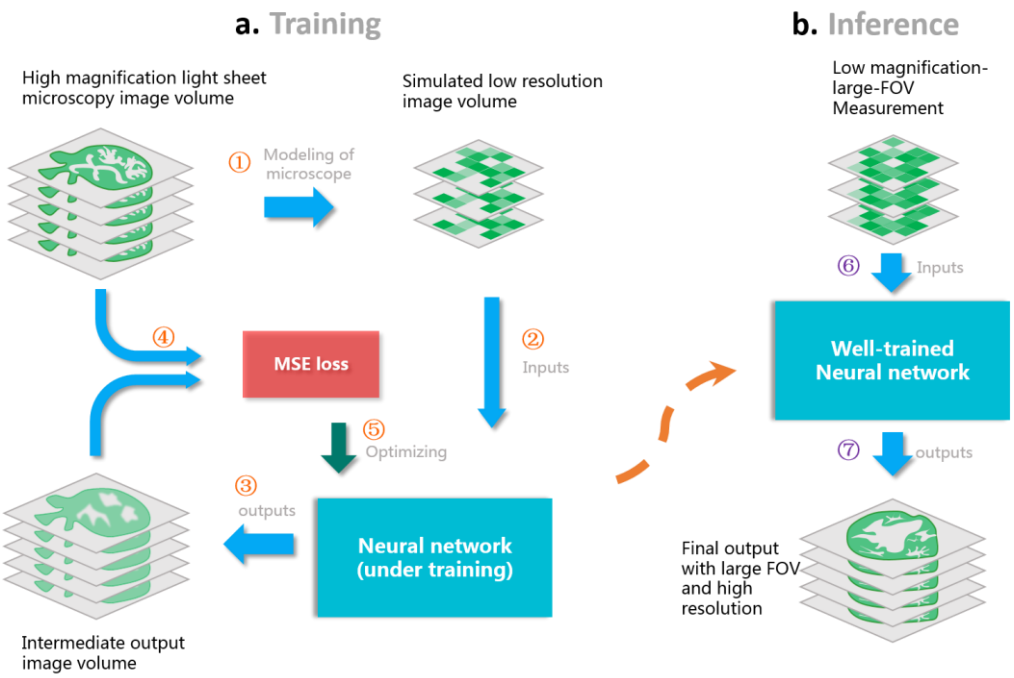

Figure 1 Overview of DVSR. (a) Training stage of DVSR. First a high resolution image volume is captured by LSFM under high magnification objective. Through a degrading model that imitates the transfer function of the optical system, high resolution volume is degraded into a simulated low resolution image volume (step 1). The low resolution simulation is then input to the neural network (step 2) to generate a intermediate output. Defined as the target output, the high resolution image volume participates in composing the loss function, which is the pixel-wise mean square error between the target output and the network intermediate output (step 4). The network parameters can be optimized through minimizing the loss function (step 5), usually by means of a gradient descent method. After a certain times of iteration, the network is regarded as well trained when the value of the loss becomes small enough. (b) Inference stage of DVSR. A large FOV but low resolution image volume is taken by LSFM under a low magnification objective, and input to the well trained network (step 5). The network immediately outputs its high resolution reconstruction of great image quality, meanwhile the large FOV remains (step 6).

Neural network structure

We use a modified residual dense network (RDN)[32] that is first proposed in 2D image super

resolution task, as our network model. RDN is a 17-layer convolutional neural network that could making full use of hierarchical features from all 2D convolutional layers. In our strategy, these 2D convolutional layers are replaced by 3D convolutional layers, which make the network capable of processing 3D inputs.

Besides, we retrofit a sub-pixel convolutional layer [35] into a 3D one, which is called sub-voxel convolutional layer hereafter, to fulfill the up-scaling from LR voxel grid to HR (Fig. 2). To illuminate how it works, we take a LR image stack in size $w * h * d * 1$ (these four dimensions represent width, height, depth and channel number respectively. Channel number is set to 1 for simplicity) as the input and up-scale it r times in each dimension (except channel dimension, which should be the same in the output and input of sub-voxel conv layer). By using r^3 different convolution kernels, our sub-voxel conv layer first expands the channel number of the input into r^3, which are further divided into $d * r$ groups. Within each group, the channels are fused to the width and height dimension to form a single slice of size $(w * r) * (h * r)$. Together $d * r$ slices from all of the groups compose a whole image volume of size $(w * r) * (h * r) * (d * r)$.

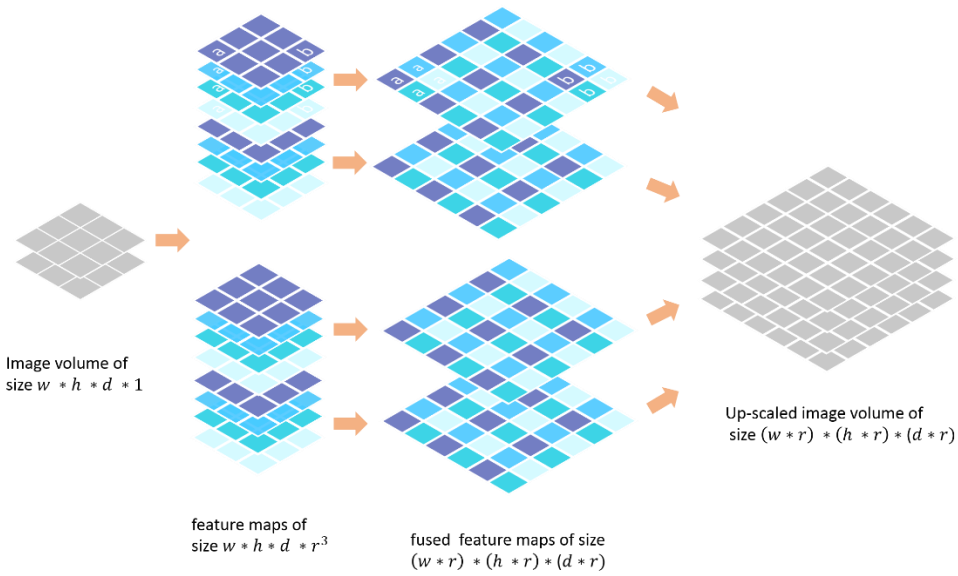

Figure 2 Sub-voxel Convolutional Layer. The input of sub-voxel conv layer is a 3-D image volume. To up-scale it r times in width, height and depth, sub-voxel conv layer first extracts $w * h * d * r^3$ feature maps from the input, and divides them into $d * r$ groups. Feature maps in one group are then fused together into a single slice to expand lateral size. Finally $d * r$ slices composes a interpolated image stack of size $(w * r) * (h * r) * (d * r)$.

Validating DVSR on simulated LSFM zebrafish heart images

We first validate DVSR on simulated light sheet images of zebrafish heart. The 3-D image degrading model is used for the generation of both training dataset and validating images. Specifically, we captured a series of fluorescent images of transgenic adult zebrafish hearts (*tg* cmlc2 : gfp) by a selective plane illumination microscope (SPIM) with using an x4 magnification setup (10 µm light-sheet illumination and 4X/0.13 detection objective). Then a down-sampling (factor of 4) in both lateral and axial dimensions, followed by addition of Gaussian and Poisson noise were applied to

these measurements to create x1 simulation images. The neural network was thereafter trained using the x4 measurements as HR targets and their x1 simulations as LR inputs. Next, we applied the well-trained network to reconstruct another x1 simulation (Fig. 3a) that was excluded from the training dataset. Two volume-of-interests (Fig. 3b1 and c1) are cropped out for a better comparison with their corresponding HR views (Fig.3 b2 and c2) and DVSR reconstructions (Fig. 3b3 and c3). Note that each vignette cubic (gray scale) is composed of 3 slices extract from x-y plane (bottom), x-z plane (up left) and y-z plane (up right). Due to the decimation, views of LR are extremely blurred as compared to HR counterparts, which is a good reproduction of the scattering in LSFM of large and deep tissues. DVSR effectively reconstructs high frequency details by accurately recognizing and enhancing signals and suppressing noises and background, no matter in x-y direction or z direction. For a better illustration, we choose three linecuts at the identical signal location in c1-c3 respectively, and plot the normalized intensity along each line (Fig3. d). On the whole there are 3 peaks in HR (green) and DVSR reconstruction (blue) signals, but only 2 in LR (orange), which results from a signal decimation generally encountered under a low magnification or high scattering imaging circumstance. More quantitatively, as measuring the full width at half maximum (FWHM) of the single signal peak, the LR signal has a width of 27.4 µm, while DVSR reconstruction is 9.3 µm wide, even better than HR (15.4µm). This substantial promotion of image quality indicates that DVSR is capable of revealing decimated high frequency details and enhancing the image resolution by 3 times at least.

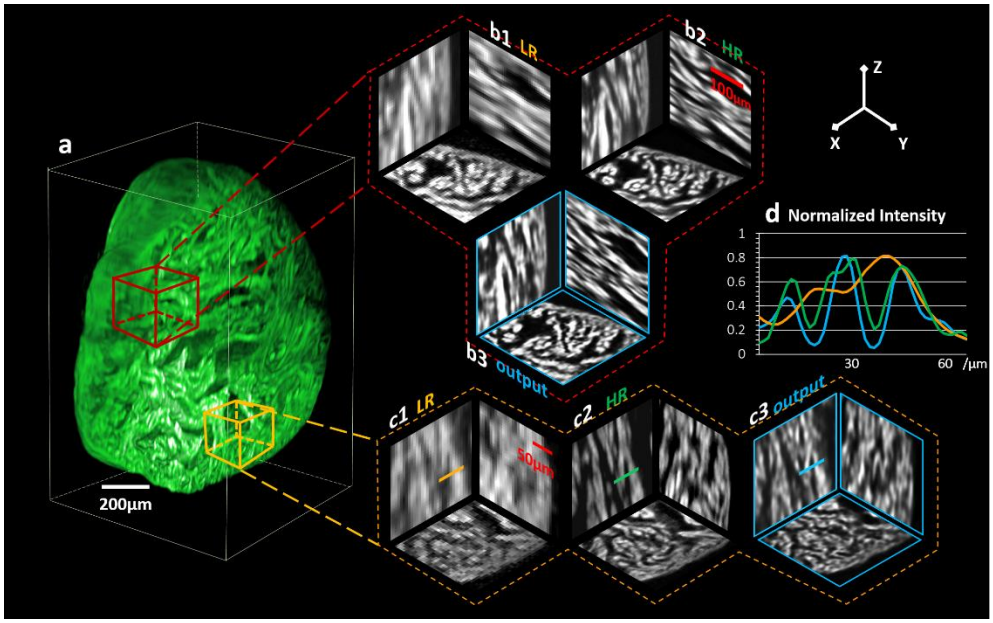

Figure 3 DVSR image of zebrafish heart. (**a**) Section view of a simulated x1 LSFM image of zebrafish heart, used as the low resolution input of the well-trained network to reconstruct. (**b1** and **c1**) Two cubic regions cropped from **a,** with 3 slices extracted from x-y, x-z and y-z plane respectively. (**b2 and c2**) The corresponding x4 high resolution views of **b1** and **c1**. (**b3** and **c3**) DVSR reconstructions of **b1** and **c1.** (**d**) profiles of linecuts through **c1, c2** and **c3**.

DVSR on LSFM mouse brain

We further tested DVSR performance on the real LSFM measurements of mouse brain. The brain tissue was first optically cleared using u-DISCO method and then imaged by a macro-view light-sheet imaging system which is based on an Olympus MVX10 microscope plus a Bessel scanning

light-sheet illumination. The HR volumes (targets) for CNN training were taken under 2-µm laser-sheet illumination in conjunction with x12.6 magnification detection. The LR inputs for training were then generated from the HR volumes through a fine-tuned degrading model. The model accurately simulates the transfer function of the optical system, allowing the simulations being close enough to the real LR measurements. The well-trained RDN network was then used to reconstruct a voxel-super-resolved volume from the LR measurements of another brain sample (Fig. 3). Due to the large size of the sample (about 2.2 * 1.7 * 3.2 mm^3), the low magnification measurement of the entire sample (6-µm illumination + x4 detection) as well as observable tissue scattering lead to a compromised imaging quality, by which the fine neuronal fibers remain very difficult to be discerned from the background (Fig. 3b1, c1, d1 and f1). This low signal-to-noise ratio (SNR) together with poor resolution of the LR measurement is posing great challenges for biological analyses. In contrast, the DVSR provides a way to computationally solve this issue. Vignette high-resolution views of DVSR reconstructions are shown in Fig. 3b2 – e2 and compared with their corresponding LR measurements. It remarkably improves the SNR of the image by suppressing background noises (b2 and c2), and three-dimensionally resolves the high-frequency details of nerve fibers (d2, e2), which can hardly be discerned in LR counterparts. A 3-D rendering of another volume-of-interest containing several neurons also indicates that DVSR reconstruction (f2) has a noticeable resolution enhancement against LR raw input (f1).

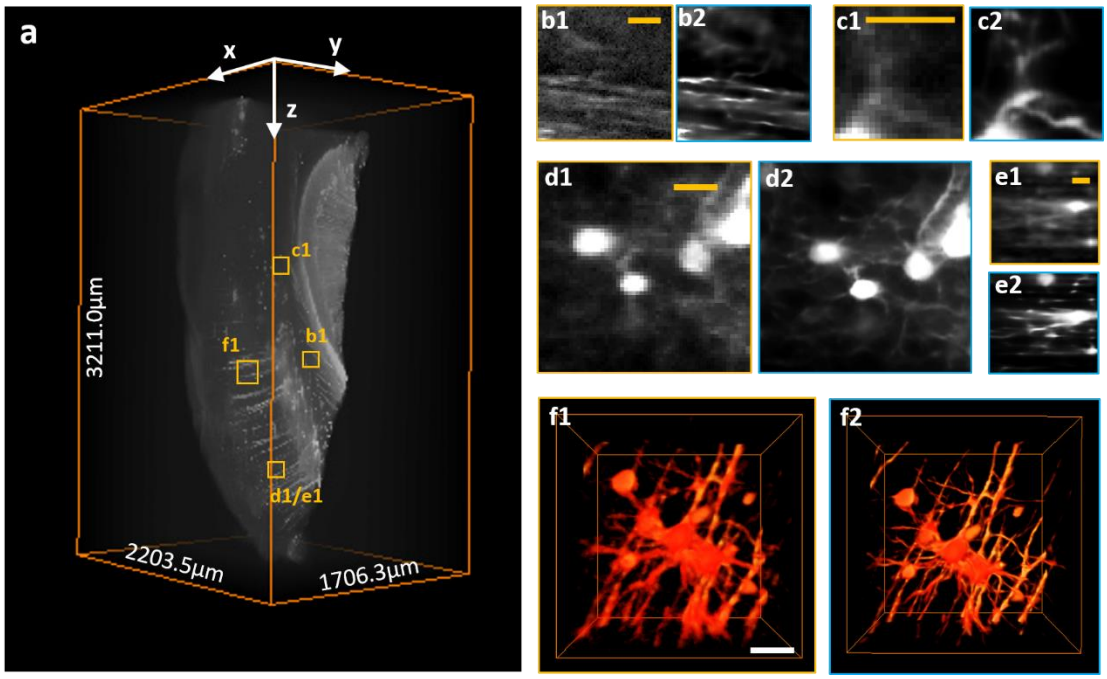

Figure 4 DVSR on Bessel LSFM mouse brain images. (**a**) 3D rendering of the x4 low resolution measurement of a mouse brain block with a volume of 2203*1706*3321 μm^3. Light sheet is scanning slice by slice along z-direction. (**b1, c1** and **d1**) Zoom-in views of regions from different selected x-y planes (i.e., slices in different tissue depth) from a. (**e1**) A low resolution y-z section from near **d1**. (**b2-e2**) The DVSR reconstructions of **b1-e1**, respectively. (**f1**) 3D rendering of a cubic region containing several neural cells, cropped from low resolution measurement **a** and (**f2**) its corresponding DVSR reconstruction. Scale bar is 20 µm in **b1-f1**.

Reliability of DVSR reconstructions

To further validate the correctness of the reconstructed mouse brain signals by DVSR, we use a computational approach[36] to quantitative map the super-resolution artifacts. This is done by first converting the super-resolution reconstructions into a diffraction-limited equivalent called the "resolution-scaled image". Using the LR input of DVSR as the reference, the pixel-wise absolute difference between the resolution-scaled image and the reference is calculated and denoted as the error map. Besides, a resolution-scaled Pearson coefficient (RSP) between the reference and resolution-scale image provides a score of image quality. RSP value ranges from -1 to 1, where higher score stands for a better reliability of the corresponding super-resolution reconstructions. Since these two metrics is designed for the evaluation of 2D images, here we use the maximum projection along z-axis of LR and reconstruction volumes to meet the data format requirements. Two groups of LR images of a mouse brain were captured with a Gaussian light-sheet illumination and used as the inputs to DVSR network. After reconstructed, the 2D maximum projection of raw inputs (Fig. 5a1, b1) and the outputs (Fig. 5a2, b2) were generated and used to compute the resolution-scale images (Fig. 5a3, b3), RSP and the error maps (Fig.5a4, b4). Positively, the RSP of both two groups has a value of over 0.9, showing a high reconstruction fidelity. Meanwhile the error maps with low but non-disappeared differences indicate that a substantial and convincible resolution enhancement by DVSR.

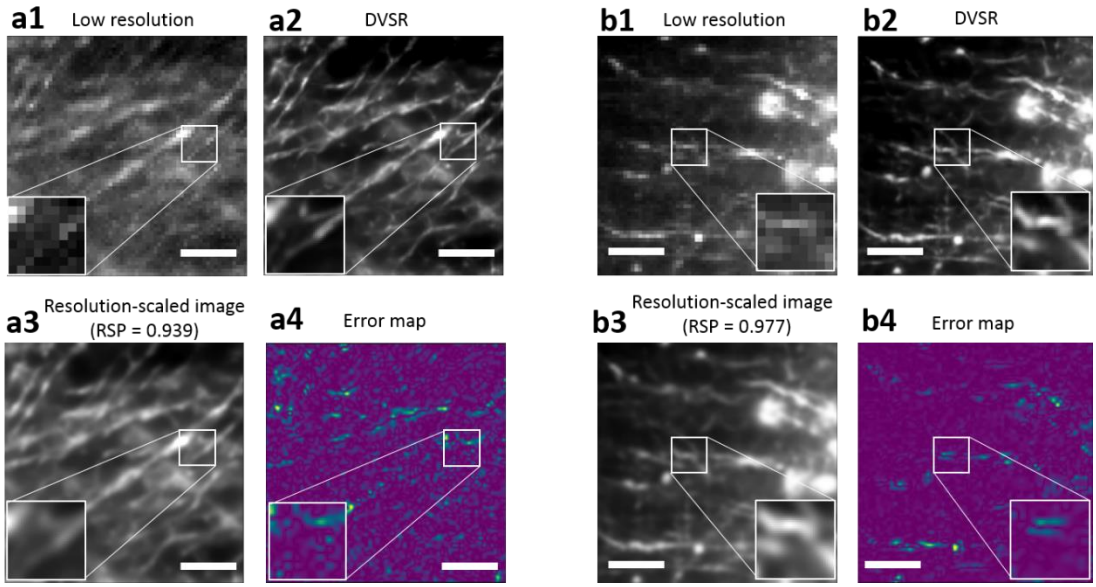

Figure 5 Quantitative mapping of DVSR artifacts. (**a1** and **b1**) Projection of x2 low resolution Gaussian LSFM measurements of a mouse brain block. (**a2** and **b2**) Projection of DVSR reconstruction using **a1** and **b1** as inputs, respectively. (**a3** and **b3**) Resolution-scaled image of a2 and b2, respectively. (**a4** and **b4**) Error map between **a1** and **a3**, **b1** and **b3** respectively. Scale bar is 50 µm.

Generalization of DVSR

DVSR is capable of efficiently reconstructing high resolution image volumes from low resolution ones based on its learned knowledge from training dataset with similar signal pattern. Naturally the question arises, that whether the DVSR network trained with one type of image data can be successfully applied to the reconstruction of another type which is very different from the training data? To figure it out, we used the DVSR network trained with Bessel LSFM images of a cleared mouse brain to recover a simulated LSFM image volume of zebrafish

heart. As shown in Fig. 6, high frequency details in the y-z section of the raw input volume (Fig. 6c, c1 and c2) is hardly recognizable. By contrast, the DVSR reconstruction (Fig. 6a, a1 and a2) presents sharp and factual structures that agree well with the HR ground truth (Fig. 6b, b1 and b2). This outstanding recovery demonstrates the high robustness of DVSR to varieties of LSFM image data.

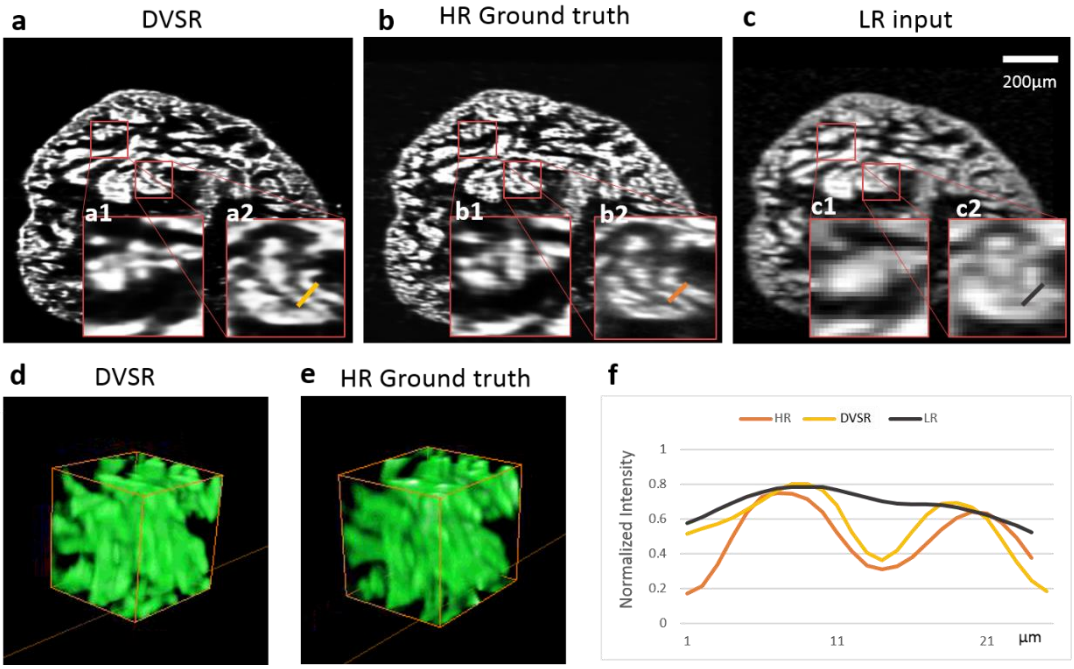

Figure 6 Generalization test of DVSR on zebrafish heart LSFM simulations. (**a**) A section of y-z plane of DVSR reconstruction, using a low resolution LSFM simulation of zebrafish heart as the input. (**b**) The section of the same area, from the corresponding high resolution ground truth. (**c**) The section of the input low resolution simulation. (**d**) 3D rendering of the cubic region near **a1** in DVSR reconstruction. (**e**) 3D rendering of the cubic region near **b1**, from high resolution ground truth. (f) Profiles of normalized intensity of pixels along linecuts in a2, b2 and c2.

Methods

LSFM Image acquisition for adult zebrafish heart and mouse brain

We used a simple selective plane illumination light sheet microscope (SPIM) which is constructed by ourselves, to carried the volumetric imaging of zebrafish hearts. The size of uniform illumination range of the hyperbolic laser-sheet is proportional to the thickness of laser-sheet, which can be further tuned by an adjustable slit. In our demonstration, the axial extent (thickness at beam waist) of the laser-sheet is ~10 μm, generating a sufficiently long range to illuminate the adult zebrafish heart with size around 1.5 by 1.5 by 1.5 mm. A 3-D motorized stage can move the sample at x-y plane, scan it along z direction, and rotate it along y direction with accurate incremental angle. The plane-illuminated heart is three-dimensionally imaged under x4 magnification with a scanning step-size 3 μm, yielding LSFM volume with unit voxel size 1.625 by 1.625 by 3 μm.

We used a home-built Bessel scanning light-sheet microscope to image the mouse brain tissues. The system is based on a macro-view microscope (Olympus MVX10, x1.26 to x12.6) integrated with a tunable thin Bessel light-sheet illumination (2 μm to 6 μm). Before imaging, the completely opaque mouse brain tissue (P30, *Tg* thy1-GFP) was optically cleared using u-DISCO method[37].

The HR and LR images were taken under x12.6 plus 2-µm plane illumination, and x4 magnification plus 6-µm plane illumination, respectively.

Data pre-processing

To make sure that the DVSR network could learning from targets of high quality, HR LSFM image volumes used as the target in training stage should have a SNR as high as possible, which is merely achieved due to the inevitable light scattering. To address this, we applied a rolling ball background subtraction (ImageJ) to decrease the intensity of background noises. The raw HR volumes with background noises were used for generating LR simulations of which the SNR were even worse. The background subtracted version of HR and the generated LR were then cropped into small 3D image blocks, where HR blocks have a dimension of 256 pixel * 256 pixel * 64 pixel and LR is of 64 pixel * 64 pixel * 16 pixel in size. To further augment the dataset, we also applied image rotation, transformation and scaling to these blocks. At last over 10000 pairs of blocks were generated to compose the training dataset.

Programming implementation and network training.

Our neural network is built up on the Tensorflow framework and trained on an Inspur® server with a Nvidia Tesla P100 graphic card installed. The training process lasted about 12 hours with a dataset containing about 10000 pairs of LR and HR image block as mentioned above.

Image reconstruction

In the inference phase after network been well-trained, the experimentally captured LR LSFM images were also cropped into small blocks with the same size as LR training blocks, and then input to the DVSR network to reconstruct one by one. Note that we also have a parallel version of inference that process several blocks simultaneously, where the number of blocks can be adjusted according to the memory size of the computer. Afterwards, the reconstructed blocks were tiled together as a whole image volume, which possesses a large FOV and high resolution.

Conclusion

We introduced DVSR, an artificial neural network based voxel-super-resolution approach that is capable of computationally improving the quality of LSFM data. While applied to a low resolution image volume acquired with conventional LSFM, this method significantly enhances the image resolution by recovering high frequency details which were decimated in low resolution raw image as well as suppressing background noises caused by light scattering in deep tissue. We utilized and reformed a novel neural network model, residual dense net, to propose our 3D RDN for 3 dimensional image super resolution. We also came up with Sub-voxel convolutional layer, a customized up-sampling mechanism for deep learning based voxel-super-resolution tasks. As all other deep learning approaches do, DVSR requires a training stage to establish its ability of mapping from low resolution inputs to high resolution outputs. We took advantage of the image degrading model to generate simulated training dataset, thus avoided complex 3D image registration between the low resolution image volumes and their high resolution counterparts. At inference stage, the performance of DVSR was tested on simulated LSFM images of adult zebrafish heart and real LSFM measurements of mouse brain block. The presented remarkable resolution enhancement and high fidelity of reconstruction on these data proves DVSR an efficient and reliable technique for 3D image super resolution, which greatly increases the throughput of a LSFM system meanwhile does not necessitate any retrofits to the existing hardware setup.

Reference

1. Keller, P.J., et al., *Reconstruction of Zebrafish Early Embryonic Development by Scanned Light Sheet Microscopy.* Science, 2008. **322**(5904): p. 1065-1069.
2. Ahrens, M.B., et al., *Whole-brain functional imaging at cellular resolution using light-sheet microscopy.* Nature Methods, 2013. **10**(5): p. 413.
3. Verveer, P.J., et al., *High-resolution three-dimensional imaging of large specimens with light sheet-based microscopy.* Nature Methods, 2007. **4**(4): p. 311-313.
4. Huisken, J., et al., *Optical Sectioning Deep inside Live Embryos by Selective Plane Illumination Microscopy.* Science, 2004. **305**(5686): p. 1007-1009.
5. Ritter, J.G., et al., *Light Sheet Microscopy for Single Molecule Tracking in Living Tissue.* Plos One, 2010. **5**(7): p. e11639.
6. Tomer, R., et al., *Quantitative high-speed imaging of entire developing embryos with simultaneous multiview light-sheet microscopy.* Nature Methods, 2012. **9**(7): p. 755.
7. Keller, P.J., et al., *Fast, high-contrast imaging of animal development with scanned light sheet-based structured-illumination microscopy.* Nature Methods, 2010. **7**(8): p. 637.
8. Chen, B.C., et al., *Lattice Light Sheet Microscopy: Imaging Molecules to Embryos at High Spatiotemporal Resolution.* Science, 2014. **346**(6208): p. 1257998.
9. Keller, P.J., et al., *Reconstruction of zebrafish early embryonic development by scanned light sheet microscopy.* Science, 2008. **322**(5904): p. 1065-1069.
10. Keller, P.J. and E.H. Stelzer, *Quantitative in vivo imaging of entire embryos with Digital Scanned Laser Light Sheet Fluorescence Microscopy.* Current Opinion in Neurobiology, 2008. **18**(6): p. 624.
11. Fei, P. *Large scale, high-throughput neuro imaging with voxel super-resolved light-sheet microscopy*. in *The International Multidisciplinary Conference on Optofluidics*. 2017.
12. Liu, S., et al., *Three-dimensional, isotropic imaging of mouse brain using multi-view deconvolution light sheet microscopy.* Journal of Innovative Optical Health Sciences, 2017. **10**(5).
13. Xie, X., et al., *Combination Light-Sheet Illumination with Super-Resolution Three-Dimensional Fluorescence Microimaging.* Chinese Journal of Lasers, 2018. **45**(3): p. 0307006.
14. Zheng, G., R. Horstmeyer, and C. Yang, *Wide-field, high-resolution Fourier ptychographic microscopy.* Nature Photonics, 2013. **7**(9): p. 739-745.
15. Zhong, J., et al., *Computational illumination for high-speed in vitro Fourier ptychographic microscopy.* Optica, 2015. **2**(10): p. 904.
16. Sharpe, J., et al., *Optical projection tomography as a tool for 3D microscopy and gene expression studies.* Science, 2002. **296**(5567): p. 541-5.
17. Nelson, A.C., et al., *Three-dimensional imaging of single isolated cell nuclei using optical projection tomography.* Optics Express, 2005. **13**(11): p. 4210-23.
18. Choi, W., et al., *Tomographic phase microscopy. Quantitative imaging of living cells.* 2007.
19. Choi, W., et al., *Extended depth of focus in tomographic phase microscopy using a propagation algorithm.* Optics Letters, 2008. **33**(2): p. 171-3.
20. Sung, Y., et al., *Optical diffraction tomography for high resolution live cell imaging.* Optics Express, 2009. **17**(1): p. 266-77.
21. Fangyen, C., et al., *Video-rate tomographic phase microscopy.* Journal of Biomedical Optics,

2011. **16**(1): p. 011005.

22. Debailleul, M., et al., *Holographic microscopy and diffractive microtomography of transparent samples.* Measurement Science & Technology, 2013. **19**(7): p. 184-187.
23. Fei, P., *A Kind of Three Dimensional Voxel Super-Resolved Light Sheet Microscopy.* 2014.
24. Fei, P., et al., *Sub-voxel light-sheet microscopy for high-resolution, high-throughput volumetric imaging of large biomedical specimens.* 2018.
25. Rivenson, Y., et al., *Deep learning enhanced mobile-phone microscopy.* Acs Photonics, 2017.
26. Ozcan, A., et al., *Deep learning microscopy.* 2017.
27. Zhang, H., et al., *High-throughput, high-resolution Generated Adversarial Network Microscopy.* 2018.
28. Hongda Wang, Y.R., Yiyin Jin, Zhensong Wei, Ronald Gao, Harun and L.A.B. Günaydın, Aydogan Ozcan, *Deep learning achieves super-resolution in fluorescence microscopy.* BioRxiv, 2018. **309641**.
29. Ouyang, W., et al., *Deep learning massively accelerates super-resolution localization microscopy.* Nature Biotechnology, 2018. **36**(5).
30. Recht, N.B.E.J.H.B.B., *DeepLoco: Fast 3D Localization Microscopy Using Neural Networks.* BioRxiv, 2018. **236463**.
31. Nehme, E., et al., *Deep-STORM: super-resolution single-molecule microscopy by deep learning.* 2018.
32. Zhang, Y., et al., *Residual Dense Network for Image Super-Resolution.* 2018.
33. Ledig, C., et al., *Photo-Realistic Single Image Super-Resolution Using a Generative Adversarial Network.* 2016.
34. Lim, B., et al. *Enhanced Deep Residual Networks for Single Image Super-Resolution*. in *Computer Vision and Pattern Recognition Workshops*. 2017.
35. Shi, W., et al. *Real-Time Single Image and Video Super-Resolution Using an Efficient Sub-Pixel Convolutional Neural Network*. in *IEEE Conference on Computer Vision and Pattern Recognition*. 2016.
36. Culley, S., et al., *Quantitative mapping and minimization of super-resolution optical imaging artifacts.* Nature Methods, 2018.
37. Pan, C., et al., *Shrinkage-mediated imaging of entire organs and organisms using uDISCO.* Nature Methods, 2016. **13**(10): p. 859-867.